PCCP

PAPER

View Article Online
View Journal | View Issue

Cite this: *Phys. Chem. Chem. Phys.*, 2014, **16**, 24747

Surface sites on Pt–CeO_2 mixed oxide catalysts probed by CO adsorption: a synchrotron radiation photoelectron spectroscopy study

Armin Neitzel,[a] Yaroslava Lykhach,*[a] Tomáš Skála,[b] Nataliya Tsud,[b] Mykhailo Vorokhta,[b] Daniel Mazur,[b] Kevin C. Prince,[cd] Vladimír Matolín[b] and Jörg Libuda[ae]

Received 28th July 2014,
Accepted 6th October 2014

DOI: 10.1039/c4cp03346a

www.rsc.org/pccp

By means of synchrotron radiation photoemission spectroscopy, we have investigated Pt–CeO_2 mixed oxide films prepared on CeO_2(111)/Cu(111). Using CO molecules as a probe, we associate the corresponding surface species with specific surface sites. This allows us to identify the changes in the composition and morphology of Pt–CeO_2 mixed oxide films caused by annealing in an ultrahigh vacuum. Specifically, two peaks in C 1s spectra at 289.4 and 291.2 eV, associated with tridentate and bidentate carbonate species, are formed on the nanostructured stoichiometric CeO_2 film. The peak at 290.5–291.0 eV in the C 1s spectra indicates the onset of restructuring, *i.e.* coarsening, of the Pt–CeO_2 film. This peak is associated with a carbonate species formed near an oxygen vacancy. The onset of cerium oxide reduction is indicated by the peak at 287.8–288.0 eV associated with carbonite species formed near Ce^{3+} cations. The development of surface species on the Pt–CeO_2 mixed oxides suggests that restructuring of the films occurs above 300 K irrespective of Pt loadings. We do not find any adsorbed CO species associated with Pt^{4+} or Pt^{2+}. The onset of Pt^{2+} reduction is indicated by the peak at 286.9 eV in the C 1s spectra due to CO adsorption on metallic Pt particles. The thermal stability of Pt^{2+} in Pt–CeO_2 mixed oxide depends on Pt loading. We find excellent stability of Pt^{2+} for 12% Pt content in the CeO_2 film, whereas at a Pt concentration of 25% in the CeO_2 film, a large fraction of the Pt^{2+} is converted into metallic Pt particles above 300 K.

1. Introduction

Fuel cells (FCs) attract significant attention as environmentally friendly power sources producing electricity from chemical fuels, *e.g.* hydrogen, methanol. Platinum is the most active catalytic material used in FCs. Presently, the high cost of platinum is the main factor limiting the large-scale application of fuel cell technology. Therefore, tremendous effort is put into the development of new catalytic materials with low noble metal content.[1–7]

The atomically dispersed supported noble metal catalysts represent a new generation of cost-effective catalytic materials.[1–7] The efficient use of noble metals requires the noble metal atoms to be anchored at the surface of the catalyst. The thermal stability of such systems must be high enough to prevent sintering and dissolution of the noble metal into the bulk. Recently, we demonstrated that nanostructured cerium oxide films expose {100} nanofacets[8] which can stabilize Pt atoms in the form of Pt^{2+} ions.[5] The {100} nanofacets expose square oxygen pockets in which Pt^{2+} ions are strongly bound. The adsorption energy of Pt^{2+} in the square oxygen pockets estimated by density functional calculations is large and explains the outstanding thermal stability of the Pt–CeO_2 films.[5] In order to maintain this high stability, the number of Pt atoms in the Pt–CeO_2 films must not exceed the number of available square oxygen pocket sites. However, thermal treatment of the films often triggers restructuring of the catalyst, which may lead to a decrease in the density of the stable sites. As a result it could lead to the formation of Pt particles.

Pt–CeO_2 mixed oxides that contain ionic Pt species can be prepared by several methods, including solution combustion,[3,4,9,10] r.f. magnetron sputtering,[11–13] and co-deposition of Pt and Ce in the oxygen atmosphere.[5] The composition and thermal stability of these materials depend strongly on the surface structure and

[a] *Lehrstuhl für Physikalische Chemie II, Friedrich-Alexander-Universität Erlangen-Nürnberg, Egerlandstrasse 3, 91058 Erlangen, Germany. E-mail: yaroslava.lykhach@fau.de*
[b] *Charles University, Faculty of Mathematics and Physics, Department of Surface and Plasma Science, V Holešovičkách 2, 18000 Prague, Czech Republic*
[c] *Elettra-Sincrotrone Trieste SCpA, Strada Statale 14, km 163.5, 34149 Basovizza-Trieste, Italy*
[d] *IOM, Strada Statale 14, km 163.5, 34149 Basovizza-Trieste, Italy*
[e] *Erlangen Catalysis Resource Center, Friedrich-Alexander-Universität Erlangen-Nürnberg, Egerlandstrasse 3, 91058 Erlangen, Germany*

Pt concentration.[5] Often formation of Pt^{2+} is also accompanied by generation of Pt^{4+} and Pt^0 species. Therefore, analysis of surface sites is important to understand and tune the stability of Pt–CeO_2 films. CO is among the most common probe molecules in heterogeneous catalysis,[14–16] typically in combination with infrared (IR) absorption spectroscopy. In many cases, however, the assignment of complex vibrational spectra is not straightforward. CO and CO_2 adsorption on ceria represents a particularly complex case, with a broad range of surface species that can be formed, *e.g.* monodentate, bidentate, tridentate, bridging, and chelating carbonates, carboxylates and carbonites.[17–26] In such cases the identification of the species and their adsorption sites is often assisted by density functional calculations.[25–29] In particular, interaction of CO molecules with planar CeO_2(111), CeO_2(110), and CeO_2(100) surfaces[27] as well as CeO_2 particles[28] has been modelled by density functional theory (DFT). It has been reported that CO reacts with CeO_2(111) rather weakly and does not yield carbonates.[26,27,29] In contrast, formation of bridged carbonates has been predicted on (110) and (100) surfaces of CeO_2, accompanied by reduction of Ce^{4+} to Ce^{3+}.[27] The authors concluded that several parameters control the formation of carbonates, *i.e.* the O–O distance, coordination of oxygen atoms, and energy of oxygen vacancy formation. Vayssilov *et al.*[28] pointed out that nanosized particles of cerium oxide show higher reactivity than the flat surfaces. This can be rationalized by the strongly reduced energy of oxygen vacancy formation.[30–32] Interestingly, the comprehensive DF modeling of CO interaction with CeO_2 nanoparticles revealed that the carbonates adsorbed in three possible tridentate configurations are more stable than the bidentate species. The differences between the tridentate carbonates are related to the coordination of their oxygen atoms to cerium cations.[28]

In contrast to IR spectroscopy, high resolution synchrotron radiation photoelectron spectroscopy (SRPES) allows direct determination of the oxidation state of Pt as well as the site-specific assignment of the adsorbed surface species. For instance, CO molecules adsorbed on different Pt surface sites can be identified by the binding energy of the corresponding features in the C 1s spectrum.[33–36] The carbonate and carboxylate species can also be observed by means of SRPES under UHV conditions.[22,23,37,38]

In the present paper we employ SRPES to monitor the reactivity of Pt–CeO_2 films towards CO. In parallel, we use resonant photoemission spectroscopy (RPES) to monitor the oxidation state of Ce cations during annealing. CO as a probe molecule provides not only information on the reactive surface sites on CeO_2 and Pt–CeO_2, but in parallel allows us to monitor structural rearrangements and formation of metallic Pt particles that may occur upon annealing of the films in UHV.

2. Experimental

High-resolution SRPES was performed at the Materials Science Beamline (MSB), Elettra synchrotron light facility in Trieste, Italy. The MSB, with a bending magnet source provides synchrotron light in the energy range of 21–1000 eV. The UHV end-station (base pressure 1×10^{-10} mbar) is equipped with a multichannel electron energy analyzer (Specs Phoibos 150), a rear view Low Energy Electron Diffraction (LEED) optics, a sputter gun (Ar), and a gas inlet system. The basic setup of the chamber includes a dual Mg/Al X-ray source.

Two samples containing 12% and 25% of Pt in the Pt–CeO_2 oxide film were prepared on a well-ordered CeO_2(111) buffer layer grown on a single crystal Cu(111) substrate. Cu(111) (MaTecK GmbH, 99.999%) was cleaned by several cycles of Ar^+ sputtering (300 K, 60 min) and annealing (723 K, 5 min) until no traces of carbon or any other contaminant were found in the photoelectron spectra. Then, an epitaxial CeO_2(111) layer was deposited onto the clean Cu(111) substrate by physical vapor deposition (PVD) of Ce metal (Goodfellow, 99.99%) in an oxygen atmosphere ($p_{O_2} = 5 \times 10^{-5}$ Pa, Linde, 99.999%) at 523 K. This preparation method[39] yielded a continuous, stoichiometric CeO_2(111) film with a thickness of 1.2 nm as determined from the attenuation of the Cu $2p_{3/2}$ intensity. In the next step, the mixed Pt–CeO_2 films were prepared by means of simultaneous PVD of Ce and Pt (Goodfellow, 99.99%) metals in an oxygen atmosphere ($p_{O_2} = 5 \times 10^{-5}$ Pa) onto the CeO_2(111)/Cu(111) at 110 K. The low deposition temperature results in a growth of Pt–CeO_2 nanoparticles on the CeO_2(111) film.[5]

The Pt concentration of 12% and 25% in the volume of the mixed layers was achieved by using Pt/Ce deposition rate ratios of 1/7 and 1/3, respectively. The deposition rate ratios were determined from the ratios of nominal thicknesses of Pt to CeO_2 deposited during the same period of time. Both Pt–CeO_2/CeO_2(111) samples maintained a nominal thickness of the Pt–CeO_2 layer of 0.3 nm.

During the course of experiments, both Pt–CeO_2/CeO_2(111) samples were annealed at different temperatures for 5 min followed by cooling to 110 K. At 110 K, the Pt–CeO_2/CeO_2(111) samples were exposed to 50 L of CO (Linde 99.98%). Additionally, a reference Pt-free CeO_2 thin film was deposited by PVD of Ce in an oxygen atmosphere ($p_{O_2} = 5 \times 10^{-5}$ Pa) onto the CeO_2(111)/Cu(111) surface at 110 K. The thickness of the Pt-free CeO_2 thin film was 0.4 nm.

The C 1s, O 1s, and Pt 4f spectra were acquired with photon energies of 410, 650, and 180 eV, respectively. The binding energies in the spectra acquired with synchrotron radiation were calibrated with respect to the Fermi level. Additionally, Al Kα radiation (1486.6 eV) was used to measure O 1s, C 1s, Ce 3d, Pt 4f, and Cu $2p_{3/2}$ core levels. All spectra were acquired at constant pass energy and at an emission angle for the photoelectrons of 20° or 0° with respect to the sample normal, while using the X-ray source or synchrotron radiation, respectively. All spectral components were fitted with a Voigt profile. Pt 4f spectra were fitted by doublet peaks with a spin orbit split of 3.3 eV and a fixed branching ratio of 1.33. Cu 3p spectra were fitted by a doublet with a fixed spin orbit splitting of 2.42 eV and a fixed branching ratio of 2. A Shirley background was subtracted before fitting C 1s spectra, whereas a combination of a linear and Shirley background was subtracted from Pt 4f spectra.

Valence band spectra were acquired at three different photon energies, 121.4, 124.8, and 115.0 eV, that correspond to the

resonant enhancements in Ce^{3+}, Ce^{4+} ions, and to off-resonance conditions, respectively. Analysis of the spectra obtained with these photon energies forms the basis of RPES.[32,40] The ratio between the corresponding resonant intensities, $D(Ce^{3+})/D(Ce^{4+})$, is a direct measure of the degree of reduction of cerium oxide. All SRPES data were processed using KolXPD fitting software.[41] The values of total spectral resolution were 1 eV (Al Kα), 200 meV ($h\nu$ = 115–180 eV), 400 meV ($h\nu$ = 410 eV) and 650 meV ($h\nu$ = 650 eV). During the experiment, the sample temperature was controlled by a DC power supply passing a current through Ta wires holding the sample. Temperatures were monitored by a K-type thermocouple attached to the back of the sample.

3. Results and discussion

3.1 The adsorption of CO on a Pt-free CeO_2 reference sample

C 1s spectra obtained from the reference Pt-free CeO_2 sample are presented in Fig. 1a. The sample was annealed to different temperatures, cooled again to 110 K and exposed to 50 L CO. For each annealing temperature we show a spectrum taken before (black) and after (green) CO exposure. The C 1s spectrum from the as-prepared sample exhibits three peaks at 289.4 (A), 291.2 (B), and 285.0 eV (E) (top, black).

Exposure to 50 L of CO results in an increase of the peak (B) but has almost no influence on the intensities of peaks (A) and (E). Annealing of the sample to 150 K results in the decomposition of the species associated with peak (B) but has no effect on peaks (A) and (E). Subsequent cooling to 110 K and exposure to 50 L CO results in the re-appearance of peak (B). The intensities of the peaks (A) and (B) gradually decrease during subsequent annealing to higher temperatures and CO exposure. After annealing to 300 K, two new peaks emerge at 290.5 (C) and 288.0 (D).

Selected C 1s spectra showing the fitted components (A–E) are shown in Fig. 1b. Fig. 1c shows the evolution of the integrated C 1s intensities of peaks (A–D) as a function of annealing temperature.

Based on their binding energies the peaks (A–C) can be assigned to carbonates adsorbed at different surface sites on CeO_2.[23,37,42,43] A tentative assignment can be given based on the DFT study by Vayssilov *et al.*[28] According to this work, carbonates are formed on the CeO_2 nanoparticles predominantly in bidentate and tridentate configurations. The bidentate geometry, denoted by Vayssilov *et al.* as (1.30),[28] is obtained by binding a CO_3^{2-} entity to three Ce ions *via* one singly-coordinated and one threefold-coordinated oxygen atoms. Threefold-coordinated oxygen sites exist on {111} and {110} facets while {100} facets expose only twofold-coordinated oxygen sites. Therefore, we assume that bidentate carbonates may form at the defect sites (*e.g.* steps or edges) on {111} or {110} facets. DFT predicts a rather low stability of the bidentate carbonate which would be consistent with the disappearance of peak (B) at temperatures as low as 150 K. Alternatively, peak (B) could be assigned to physisorbed CO_2. However, the binding energy of physisorbed CO_2 on CeO_2(111) and CeO_2(100) surfaces was reported to be 292 eV, which is higher than the binding energy of peak (B) (291.2 eV).[32,44]

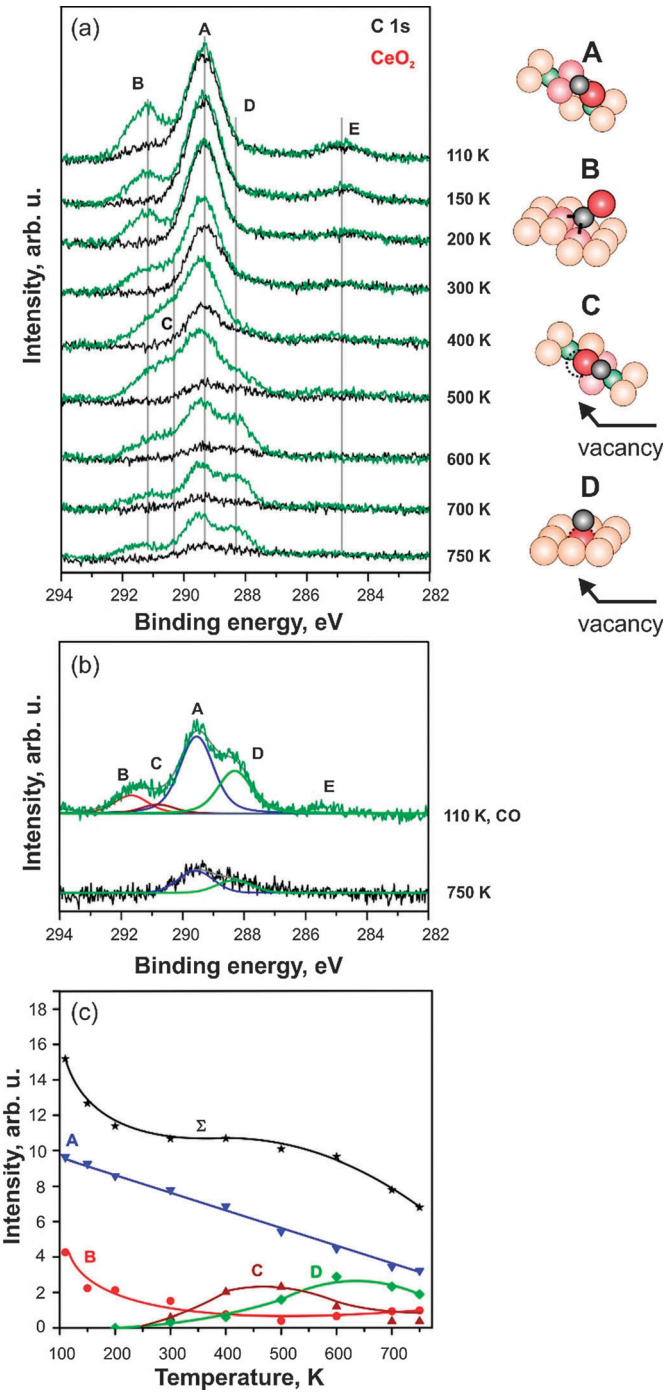

Fig. 1 (a) C 1s spectra obtained from a Pt-free CeO_2 film prepared at 110 K on CeO_2(111)/Cu(111) annealed at different temperatures (black) and exposed to 50 L of CO at 110 K (green); (b) C 1s spectra obtained from a Pt-free CeO_2 film after annealing to 750 K (black) and exposure to 50 L of CO (green) fitted with components (A–E); (c) Integrated C 1s intensities of the components (A–D) as a function of temperature. The ball and stick models illustrate possible structures of the species (A–D) on Pt-free CeO_2 film. The carbonate (C) and carbonate (D) species form by insertion into oxygen vacancy (dashed circle).

Following the work of Vayssilov *et al.*,[28] the peaks (A) and (C) can be associated with more stable carbonate species adsorbed in tridentate geometry. From the three geometries suggested by

Vayssilov *et al.*,[28] the species denoted as (1.21), *i.e.* the one that binds to three cerium cations *via* one twofold-coordinated and two singly-coordinated oxygen atoms, is formed near oxygen vacancies. The onset of partial reduction of Pt-free CeO_2 film detected by RPES above 300 K (data not shown) coincides with the emergence of peak (C). Therefore, we may tentatively attribute peak (C) to this type of carbonate.

Peak (A) could then be associated with one or both of the remaining tridentate geometries. The first species, denoted (1.2.1),[28] binds to two cerium cations *via* one twofold-coordinated and two singly-coordinated oxygen atoms. The second carbonate, denoted (1.3.1),[28] binds to three cerium cations *via* one threefold-coordinated and two singly-coordinated oxygen atoms. Albrecht *et al.*[23] reported tridentate carbonate species with a binding energy of 290.2 eV on a flat CeO_2(100) surface (exposing twofold-coordinated oxygen sites). On the other hand, the carbonates formed upon CO_2 adsorption at low temperature on a flat CeO_2(111) surface (exposing threefold-coordinated oxygen sites) have been reported to have a binding energy of 290 eV.[42] It is clear that carbonate species formed on different sites of stoichiometric CeO_2 surfaces cannot be reliably resolved by SRPES.

The assignment of the species associated with peak (D) is not straightforward. The binding energy of peak (D) (288.0 eV) is lower than the values typically reported for carbonates (289–291 eV)[23,37,42] and higher than those of inorganic carboxylates (286–287 eV) formed by CO_2 adsorption.[37,44] The species associated with peak (D) are definitely related to the presence of oxygen vacancies and Ce^{3+} cations. One possibility would be to assign the corresponding species to a surface carbonite, (CO_2^{2-}), species.[24] These species have been identified on reduced ceria after CO adsorption at room temperature.[24]

Finally, we assign the weak peak (E) at 285 eV to traces of atomic carbon on the ceria surface formed during preparation of the sample.[44] This species vanishes from the surface after annealing to temperatures higher than 400 K. The intensity of this species does not increase during annealing and CO adsorption cycles, which means that CO does not dissociate on the Pt-free CeO_2 surface under the present experimental conditions.

The changes in the morphology of the reference sample induced by stepwise annealing are related to the abundance of the adsorption sites that are associated with the peaks (A–D). We observe that the number of sites associated with the peaks (A) and (B) gradually decreases while new sites associated with the peaks (C) and (D) are formed at 300 K. However, the total density of adsorption sites decreases (see Fig. 1c). This observation indicates substantial restructuring of the film, most likely, related to surface coarsening and formation of CeO_2 particles with larger, flat facets that are less reactive towards CO.

It is noteworthy that stepwise annealing of the sample to 750 K results in a gradual shift of the peaks (A–D) to higher binding energies. This is likely to be caused by progressive reduction of cerium oxide during the course of the experiment.

3.2 The adsorption of CO on a 12% Pt–CeO_2 mixed oxide

Co-deposition of Ce and Pt in an oxygen atmosphere yields atomically dispersed Pt^{2+} and Pt^{4+} ions in a Pt–CeO_2 mixed oxide thin film.[5] The Pt 4f spectrum obtained from an as-prepared 12% Pt–CeO_2 film is shown in Fig. 2a (top, black) and 2b (bottom, black). The spectrum contains two spin–orbit doublets at binding energies of the $4f_{7/2}$ components

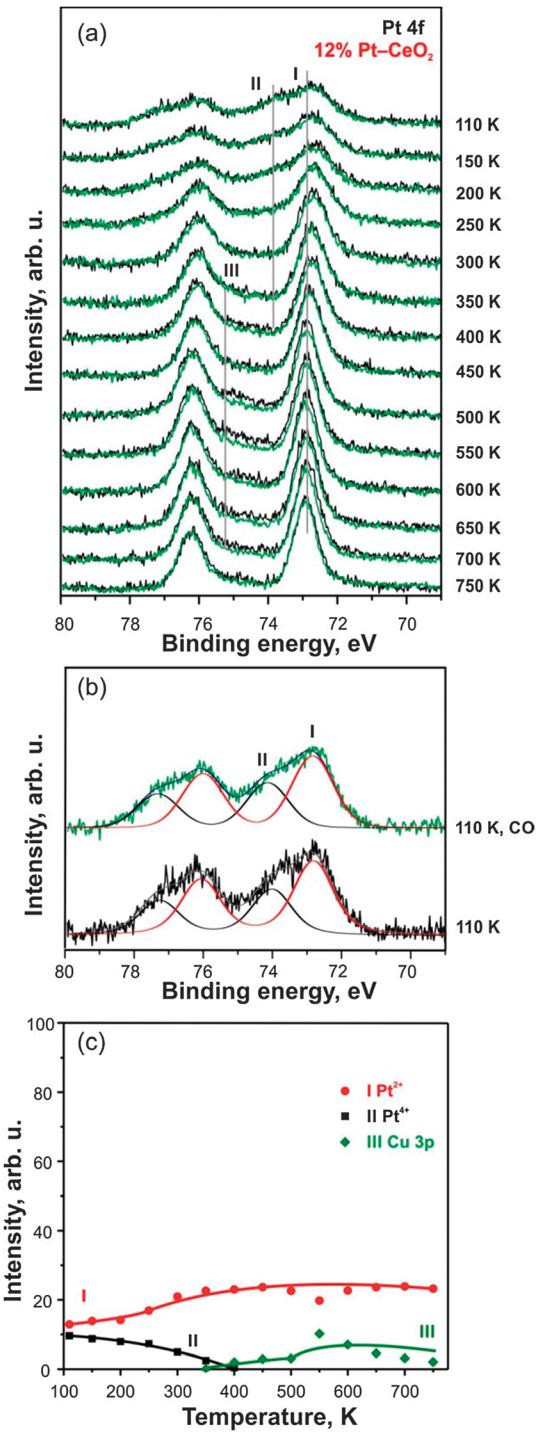

Fig. 2 (a) Pt 4f spectra obtained from a 12% Pt–CeO_2 film prepared at 110 K on CeO_2(111)/Cu(111) annealed at different temperatures (black) and exposed to 50 L of CO at 110 K (green); (b) Pt 4f spectra obtained from an as-prepared 12% Pt–CeO_2 film (black) and after exposure to 50 L of CO (green) fitted with components (I–II); (c) Integrated Pt 4f intensities of the components (I–III) as a function of temperature.

at 72.8 (I) and 74 eV (II) associated with Pt^{2+} and Pt^{4+} ions, respectively.[5]

C 1s spectra obtained from the 12% Pt–CeO_2 film after annealing to different temperatures are shown in Fig. 3a, before (black) and after (green) exposure to 50 L of CO at 110 K.

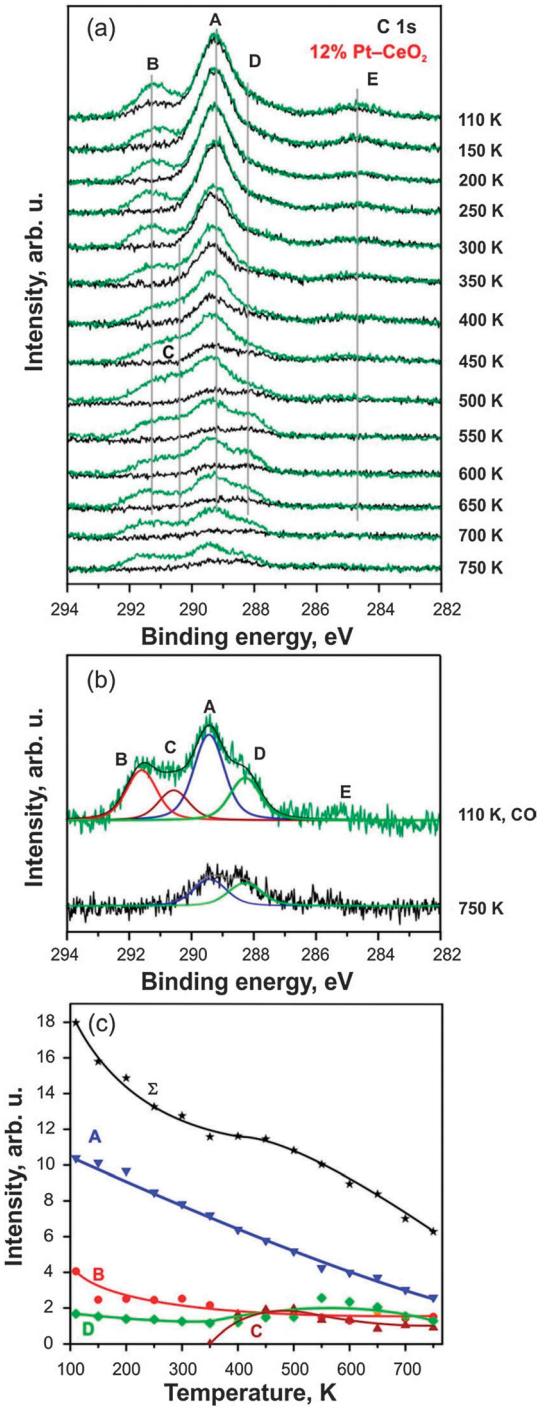

Fig. 3 (a) C 1s spectra obtained from a 12% Pt–CeO_2 film prepared at 110 K on CeO_2(111)/Cu(111) annealed at different temperatures (black) and exposed to 50 L of CO at 110 K (green); (b) C 1s spectra obtained from the 12% Pt–CeO_2 film after annealing to 750 K (black) and exposure to 50 L of CO (green) fitted with components (A–E); (c) Integrated C 1s intensities of the components (A–D) as a function of temperature.

The C 1s spectrum obtained from the as-prepared sample (top, black) consists of three peaks located at 289.3 (A), 291.3 (B), 287.8 eV (D), and a weak feature at 284.7 eV (E). These reveal a striking similarity to the reference Pt-free CeO_2 sample (Fig. 1a) discussed in Section 3.1. The only difference between the two samples is the appearance of peak (D) on the 12% Pt–CeO_2 film sample, which is detectable right from the start of the annealing series. Similar to the Pt-free CeO_2 reference sample we assign the peaks (A) and (B) to tridentate and bidentate carbonates, respectively. The small peak (E) is attributed to atomic carbon. Peak (D) is associated with the surface carbonite, related to the presence of Ce^{3+} cations. As detected by RPES, formation of Pt^{2+} ions is associated with partial reduction of the ceria cations.[5] It is noteworthy that on the as-prepared surface, peak (D) is not accompanied by peak (C) as in the case of the Pt-free CeO_2 film. This implies that the Ce^{3+} associated with the carbonite formation and the oxygen vacancies associated with the formation of the tridentate carbonate at vacancy sites are independent processes, *i.e.* they do not occur at the same sites. The emergence of peak (C) (291.0 eV) at 400 K is associated with formation of oxygen vacancies upon restructuring of the Pt–CeO_2 film.

A selected C 1s spectrum with fitted components (A–E) is shown in Fig. 3b. The development of the intensities of components (A–D) is shown in Fig. 3c. Similar to the Pt-free reference sample, we observed a decrease in the total number of adsorption sites on the 12% Pt–CeO_2 film upon annealing.

The fact that the same species are formed on both Pt-free CeO_2 and 12% Pt–CeO_2 suggests that the species formed on these surfaces are related to cerium and oxygen sites. Also, comparison of the Pt 4f spectra before and after CO adsorption at 110 K (see Fig. 2a) does not reveal any noticeable attenuation or shift of Pt^{2+} and Pt^{4+} signals. These observations suggest that CO does not adsorb on either Pt^{2+} or Pt^{4+} ions under the present experimental conditions.

Above 300 K, Pt^{4+} is quantitatively transformed into Pt^{2+}. The Pt^{2+} ions demonstrate a high thermal stability, even upon annealing to 750 K. According to our earlier studies, the Pt^{2+} ions are located in {100} nanopockets, where they resist both sintering and diffusion into deeper layers.[5]

Similar to Pt-free CeO_2, annealing of the 12% Pt–CeO_2 film above 400 K results in restructuring of the film. At 400 K, a new weak and broad doublet emerges in the Pt 4f region at 75 eV (III) due to a contribution from the Cu 3p core level. The detection of the Cu 3p signal from the Cu(111) substrate indicates restructuring of the 12% Pt–CeO_2 film, *e.g.* coarsening of the film similar to the Pt-free CeO_2 film discussed above. We note that the integrated intensity of the Cu 3p peak (III) after annealing at 750 K is smaller than that detected on the CeO_2(111)/Cu(111) buffer layer prior to deposition of the 12% Pt–CeO_2 film. Therefore, we assume that restructuring of the 12% Pt–CeO_2 film does not have a large effect on the CeO_2(111) buffer layer.

3.3 The adsorption of CO on a 25% Pt–CeO_2 mixed oxide

The Pt 4f spectrum obtained from the as-prepared 25% Pt–CeO_2 mixed oxide is shown in Fig. 4a (top, black). It contains two spin–orbit doublets at 72.5 (I) and 73.9 eV (II) associated with

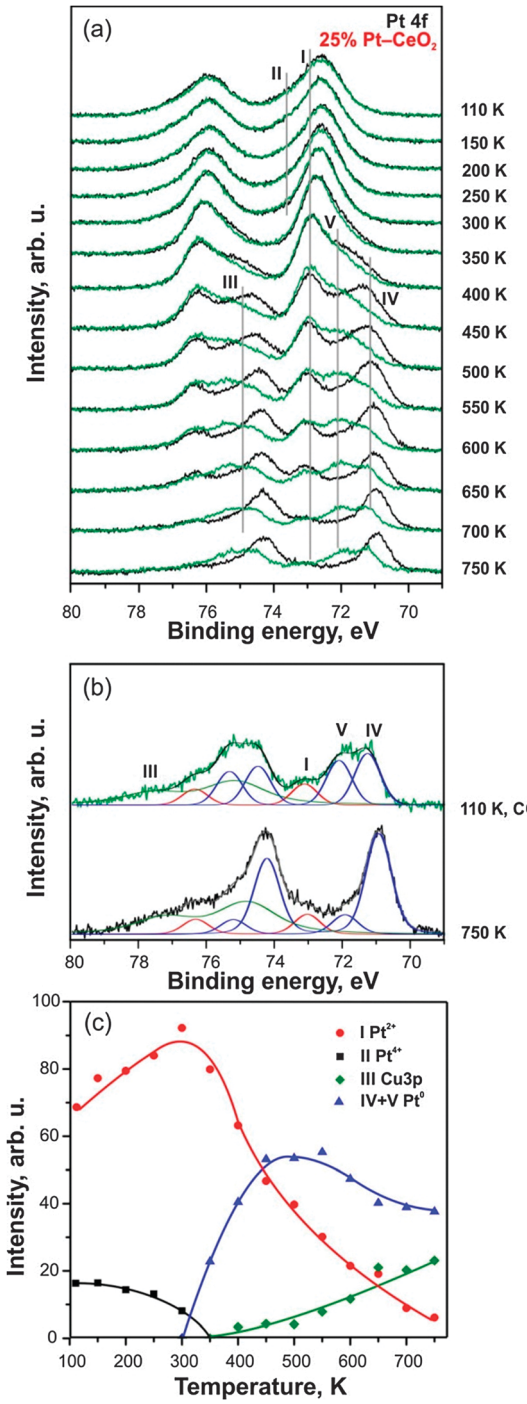

Fig. 4 (a) Pt 4f spectra obtained from a 25% Pt–CeO_2 film prepared at 110 K on CeO_2(111)/Cu(111) annealed at different temperatures (black) and exposed to 50 L of CO at 110 K (green); (b) Pt 4f spectra obtained from the 25% Pt–CeO_2 film annealed at 750 K (black) and after exposure to 50 L of CO (green) fitted with components (I–V); (c) Integrated Pt 4f intensities of the components (I–V) as a function of temperature.

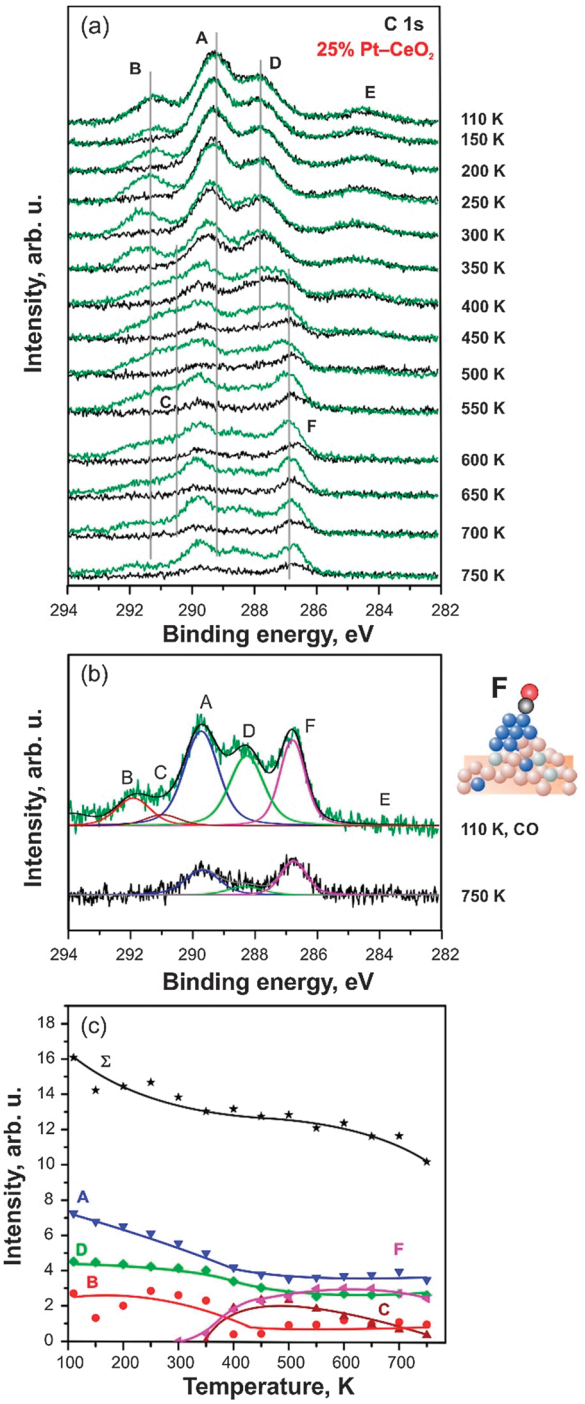

Fig. 5 (a) C 1s spectra obtained from a 25% Pt–CeO_2 film prepared at 110 K on CeO_2(111)/Cu(111) annealed at different temperatures (black) and exposed to 50 L of CO at 110 K (green); (b) C 1s spectra obtained from the 25% Pt–CeO_2 film after annealing to 750 K (black) and exposure to 50 L of CO (green) fitted with components (A–F); (c) Integrated C 1s intensities of the components (A–F) as a function of temperature. The ball and stick model illustrates the adsorption of the CO molecule in on-top geometry on a Pt particle.

Pt^{2+} and Pt^{4+}, respectively. Similar to the 12% Pt–CeO_2 film, Pt^{4+} is converted into Pt^{2+} upon annealing of the 25% Pt–CeO_2 film to 350 K.

The C 1s spectra obtained from the 25% Pt–CeO_2 film after annealing to different temperatures are shown in Fig. 5a, before and after the exposure to 50 L of CO at 110 K. Similar to the 12% Pt–CeO_2 film, we find peaks at 291.3 (B), 289.3 (A), 287.8 (D) and 284.7 eV (E). Peak (C) at 291 eV and a new peak (F)

at 286.9 eV emerge between 350 and 400 K. The C 1s spectrum with all fitted peaks is shown in Fig. 5b. The evolution of the corresponding intensities is plotted in Fig. 5c as a function of annealing temperature.

We assigned the species associated with the peaks (A–D) in Sections 3.1 and 3.2. Briefly, peak (B) was attributed to a bidentate carbonate, peak (A) to a tridentate carbonate, peak (C) to a tridentate carbonate near an oxygen vacancy, and peak (D) to a carbonite species formed in the presence of Ce^{3+}. It is noteworthy that the amount of carbonite species (D) detected on the as-prepared 25% Pt–CeO_2 is higher than on the 12% Pt–CeO_2 film. This is consistent with the higher concentration of Pt which also leads to a greater concentration of Ce^{3+} in the 25% Pt–CeO_2 film.

Further differences related to the higher Pt metal loading in the 25% Pt–CeO_2 film become apparent in the C 1s spectra after annealing above 300 K. Specifically, we observe the emergence of a new peak (F) at 286.9 eV above 350 K (see Fig. 5a). The intensity of this peak gradually gains intensity in the following annealing cycles.

The emergence of peak (F) in the C 1s spectra coincides with the occurrence of the new peak (IV) at 71.0–71.3 eV in the Pt 4f spectra after annealing of the film above 300 K. We note that the intensity of peak (IV) is attenuated upon CO adsorption at 110 K (compare Pt 4f spectra before and after CO adsorption, Fig. 4a). The attenuation correlates with the emergence of a second new peak (V) at 71.9 eV in the Pt 4f spectra after CO exposure. Thus we can attribute these spectral changes to the adsorption of CO on new Pt sites formed upon annealing.

From its binding energy, we attribute peak (IV) in the Pt 4f region 71.0–71.3 eV to metallic Pt particles. The binding energy of peak (F) in the C 1s region is consistent with assignment to CO adsorbed at on-top sites on metallic Pt particles.[33–36] Furthermore, the occurrence of peak (V) as a shifted component of peak (IV) is consistent with the core level shift due to CO adsorption.[35,36] In Fig. 4c, the summed intensities of the peaks (IV) and (V) characterize a growth of Pt particles during annealing.

Apparently, the observed reduction of Pt^{2+} to metallic Pt particles is associated with a massive restructuring of the 25% Pt–CeO_2 film. According to the development of C 1s intensities, the onset of peak (C), which indicates restructuring of the 25% Pt–CeO_2 film, takes place above 300 K. The appearance of peak (III) at 75 eV associated with Cu 3p is also consistent with the coarsening of the Pt–CeO_2 film. Unlike on the 12% Pt–CeO_2 film, however, the integrated intensity of the Cu 3p peak (III) after annealing at 750 K is larger than that detected on the CeO_2(111)/Cu(111) buffer layer prior to deposition of the 25% Pt–CeO_2 film. This observation indicates that the CeO_2(111) buffer layer also undergoes restructuring upon annealing of the 25% Pt–CeO_2 film. Interestingly, the onset of restructuring coincides with the appearance of peak (F) associated with CO adsorbed on Pt particles.

Note that metallic Pt particles do not form on the sample with low metal loading, the 12% Pt–CeO_2 film. Consequently, we conclude that the decrease of the limited density of {100} sites suitable for anchoring Pt^{2+} triggers the formation of metallic Pt particles upon thermally activated restructuring of the Pt–CeO_2 film.

4. Conclusions

The morphology and composition of Pt–CeO_2 mixed oxide films prepared on a well-ordered CeO_2(111) buffer layer on Cu(111) have been studied by means of synchrotron radiation photoelectron spectroscopy. CO has been used as a probe to monitor the development of the surface composition and sites that are exposed upon stepwise annealing of the Pt–CeO_2 mixed oxide films in UHV. The surface species formed upon CO adsorption on Pt–CeO_2 mixed oxides and Pt-free CeO_2 films have been attributed to specific surface sites and their development has been monitored.

(1) The Pt-free nanostructured CeO_2 film prepared at 110 K on a well-ordered CeO_2(111) buffer layer initially contains exclusively Ce^{4+} cations. Its surface structure allows the formation of tridentate and bidentate carbonates associated with the peaks at 289.4 and 291.2 eV in C 1s spectra, respectively. Restructuring of the film occurs above 300 K and gives rise to a partial reduction of the cerium oxide accompanied by the formation of oxygen vacancies. On the restructured film, a peak at 290.5 eV indicates the formation of tridentate carbonates formed near oxygen vacancies. At the same time carbonite species are formed near Ce^{3+} cations as indicated by a peak at 288.0 eV.

(2) On the CeO_2(111) buffer layer, Pt–CeO_2 mixed oxide films were prepared at 110 K with Pt concentration of 12% and 25%, respectively. As prepared systems contain Pt^{2+}, Pt^{4+}, Ce^{4+} and Ce^{3+}. The presence of Ce^{3+} is connected to a partial reduction of cerium oxide upon reaction with Pt during preparation. Upon annealing above 300 K, Pt^{4+} cations are converted to Pt^{2+}. The formation of carbonite species is not associated with the formation of the tridentate carbonate species at oxygen vacancies suggesting that the two species are formed at different sites.

(3) CO adsorption on the 12% Pt–CeO_2 mixed oxide film, independent of the annealing temperature (110 to 750 K) does not yield any adsorbed surface species other than those observed for the Pt-free reference system. This implies that CO does not adsorb on Pt^{2+} or on Pt^{4+} sites under UHV conditions at temperatures down to 110 K.

(4) The morphological changes induced by the annealing of the 12% and 25% Pt–CeO_2 mixed oxide are similar to the Pt-free CeO_2 film and occur above 300 K. At high Pt concentration (25% Pt–CeO_2 mixed oxide) however, restructuring triggers reduction of Pt^{2+} to metallic Pt particles. The formation of metallic Pt particles gives rise to a new peak in the C 1s spectra characteristic of molecular CO adsorption.

Acknowledgements

The authors gratefully acknowledge financial support by the European Commission in the framework of FP7 Project ''chipCAT'' (FP7-NMP-2012-SMALL-6, Grant Agreement no. 310191) and by the Ministry of Education of the Czech Republic

(LG12003 and LD13054). We acknowledge additional support from the DFG within the excellence cluster ''Engineering of Advanced Materials'' in the framework of the Excellence Initiative and within the Priority Program SPP 1708 ''Material Synthesis near Room Temperature'' as well as support from the COST Action CM1104 ''Reducible oxide chemistry, structure and functions''. Y.L., A.N., N.T., M.V., D.M., and K.C.P. thank Elettra for excellent working conditions and support.

Notes and references

1 M. Flytzani-Stephanopoulos and B. C. Gates, *Annu. Rev. Chem. Biomol. Eng.*, 2012, **3**, 545.
2 E. W. McFarland and H. Metiu, *Chem. Rev.*, 2013, **113**, 4391.
3 M. S. Hegde, G. Madras and K. C. Patil, *Acc. Chem. Res.*, 2009, **42**, 704.
4 G. Dutta, A. Gupta, U. Waghmare and M. S. Hegde, *J. Chem. Sci.*, 2011, **123**, 509.
5 A. Bruix, Y. Lykhach, I. Matolínová, A. Neitzel, T. Skála, N. Tsud, M. Vorokhta, V. Stetsovych, K. Ševčiková, J. Mysliveček, R. Fiala, M. Václavů, K. C. Prince, S. Bruyere, V. Potin, F. Illas, V. Matolín, J. Libuda and K. M. Neyman, *Angew. Chem., Int. Ed.*, 2014, **53**, 10525–10530.
6 B. T. Qiao, A. Q. Wang, X. F. Yang, L. F. Allard, Z. Jiang, Y. T. Cui, J. Y. Liu, J. Li and T. Zhang, *Nat. Chem.*, 2011, **3**, 634.
7 T. Rajesh, A. K. Rajarajan, C. S. Gopinath and R. N. Devi, *J. Phys. Chem. C*, 2012, **116**, 9526.
8 Y. Lin, Z. Wu, J. Wen, K. R. Poeppelmeier and L. D. Marks, *Nano Lett.*, 2013, **14**, 191.
9 P. Bera, A. Gayen, M. S. Hegde, N. P. Lalla, L. Spadaro, F. Frusteri and F. Arena, *J. Phys. Chem. B*, 2003, **107**, 6122.
10 P. Bera, K. C. Patil, V. Jayaram, G. N. Subbanna and M. S. Hegde, *J. Catal.*, 2000, **196**, 293.
11 V. Matolín, I. Matolínová, M. Václavů, I. Khalakhan, M. Vorokhta, R. Fiala, I. Piš, Z. Sofer, J. Poltierová-Vejpravová, T. Mori, V. Potin, H. Yoshikawa, S. Ueda and K. Kobayashi, *Langmuir*, 2010, **26**, 12824.
12 M. Vorokhta, I. Khalakhan, I. Matolínová, M. Kobata, H. Yoshikawa, K. Kobayashi and V. Matolín, *Appl. Surf. Sci.*, 2013, **267**, 119.
13 R. Fiala, I. Khalakhan, I. Matolínová, M. Václavů, M. Vorokhta, Z. Sofer, S. Huber, V. Potin and V. Matolín, *J. Nanosci. Nanotechnol.*, 2011, **11**, 5062.
14 G. Ertl, H. Knözinger, F. Schüth and J. Weitkamp, *Handbook of Heterogeneous Catalysis*, Wiley, Weinheim, 2008.
15 F. M. Hoffmann, *Surf. Sci. Rep.*, 1983, **3**, 107.
16 J. M. Chalmers and P. R. Griffiths, *Handbook of vibrational spectroscopy*, Wiley, Chichester, UK, 2001.
17 O. Pozdnyakova, D. Teschner, A. Wootsch, J. Kröhnert, B. Steinhauer, H. Sauer, L. Toth, F. C. Jentoft, A. Knop-Gericke, Z. Paál and R. Schlögl, *J. Catal.*, 2006, **237**, 1.
18 K. Mudiyanselage, H. Y. Kim, S. D. Senanayake, A. E. Baber, P. Liu and D. Stacchiola, *Phys. Chem. Chem. Phys.*, 2013, **15**, 15856.
19 N. Singhania, E. A. Anumol, N. Ravishankar and G. Madras, *Dalton Trans.*, 2013, **42**, 15343.
20 C. Li, Y. Sakata, T. Arai, K. Domen, K. Maruya and T. Onishi, *J. Chem. Soc., Faraday Trans. 1*, 1989, **85**, 929.
21 C. Li, Y. Sakata, T. Arai, K. Domen, K. Maruya and T. Onishi, *J. Chem. Soc., Chem. Commun.*, 1991, 410.
22 S. D. Senanayake, D. Stacchiola, J. Evans, M. Estrella, L. Barrio, M. Pérez, J. Hrbek and J. A. Rodriguez, *J. Catal.*, 2010, **271**, 392.
23 P. M. Albrecht, D.-e. Jiang and D. R. Mullins, *J. Phys. Chem. C*, 2014, **118**, 9042.
24 C. Binet, A. Badri, M. Boutonnet-Kizling and J.-C. Lavalley, *J. Chem. Soc., Faraday Trans.*, 1994, **90**, 1023.
25 Z. Wu, M. Li and S. H. Overbury, *J. Catal.*, 2012, **285**, 61.
26 Z. Yang, T. K. Woo and K. Hermansson, *Chem. Phys. Lett.*, 2004, **396**, 384.
27 M. Nolan and G. W. Watson, *J. Phys. Chem. B*, 2006, **110**, 16600.
28 G. N. Vayssilov, M. Mihaylov, P. S. Petkov, K. I. Hadjiivanov and K. M. Neyman, *J. Phys. Chem. C*, 2011, **115**, 23435.
29 M. Huang and S. Fabris, *J. Phys. Chem. C*, 2008, **112**, 8643.
30 A. Migani, G. N. Vayssilov, S. T. Bromley, F. Illas and K. M. Neyman, *Chem. Commun.*, 2010, **46**, 5936.
31 A. Migani, G. N. Vayssilov, S. T. Bromley, F. Illas and K. M. Neyman, *J. Mater. Chem.*, 2010, **20**, 10535.
32 G. N. Vayssilov, Y. Lykhach, A. Migani, T. Staudt, G. P. Petrova, N. Tsud, T. Skala, A. Bruix, F. Illas, K. C. Prince, V. Matolin, K. M. Neyman and J. Libuda, *Nat. Mater.*, 2011, **10**, 310.
33 B. Tränkenschuh, C. Papp, T. Fuhrmann, R. Denecke and H. P. Steinrück, *Surf. Sci.*, 2007, **601**, 1108.
34 J. G. Wang, W. X. Li, M. Borg, J. Gustafson, A. Mikkelsen, T. M. Pedersen, E. Lundgren, J. Weissenrieder, J. Klikovits, M. Schmid, B. Hammer and J. N. Andersen, *Phys. Rev. Lett.*, 2005, **95**, 2561021.
35 S. Shimizu, H. Noritake, T. Koitaya, K. Mukai, S. Yoshimoto and J. Yoshinobu, *Surf. Sci.*, 2013, **608**, 220.
36 I. Matolínová, V. Johánek, J. Mysliveček, K. C. Prince, T. Skála, M. Škoda, N. Tsud, M. Vorokhta and V. Matolín, *Surf. Interface Anal.*, 2011, **43**, 1325.
37 T. Staudt, Y. Lykhach, N. Tsud, T. Skala, K. C. Prince, V. Matolín and J. Libuda, *J. Phys. Chem. C*, 2011, **115**, 8716.
38 T. Staudt, Y. Lykhach, N. Tsud, T. Skála, K. C. Prince, V. Matolín and J. Libuda, *J. Catal.*, 2010, **275**, 181.
39 F. Šutara, M. Cabala, L. Sedláček, T. Skála, M. Škoda, V. Matolín, K. C. Prince and V. Cháb, *Thin Solid Films*, 2008, **516**, 6120.
40 V. Matolin, I. Matolinova, L. Sedlacek, K. C. Prince and T. Skala, *Nanotechnology*, 2009, **20**, 215706.
41 J. Libra, KolXPD: Spectroscopy data measurement and processing, http://www.kolibrik.net/science/kolxpd/.
42 S. D. Senanayake and D. R. Mullins, *J. Phys. Chem. C*, 2008, **112**, 9744.
43 P. M. Albrecht and D. R. Mullins, *Langmuir*, 2013, **29**, 4559.
44 Y. Lykhach, T. Staudt, R. Streber, M. P. Lorenz, A. Bayer, H. P. Steinrück and J. Libuda, *Eur. Phys. J. B*, 2010, **75**, 89.

